TRANSIENT ANALYSIS OF A LINEAR INDUCTION MACHINE USING THE d,q POLE-BY-POLE MODEL

T.A. Nondahl T.A. Lipo

General Electric Co.
Schenectady, NY

ABSTRACT

An evaluation of transient as well as steady-state behavior of linear induction machines (LIM's) is essential for high horsepower applications. The pole-by-pole model, a low order coupled circuit model derived for arbitrary excitation, provides a unique method of analyzing such behavior. In this paper a computer simulation algorithm suitable for either analog or digital computation is derived. To illustrate the flexibility of the approach practical application considerations such as acceleration response, behavior with an inverter supply and the effect of frequency step changes and SCR failure are modeled. Where feasible, computed waveforms are compared to test measurements from an actual prototype machine.

1. INTRODUCTION

The pole-by-pole model [1] portrays linear induction machines (LIM's) in a way radically different from more established field analysis methods [2-6] by forming a coupled circuit model similar to that widely used in rotary induction machine analysis [7]. The key assumption in the pole-by-pole model is the premise that, because of the finite length of the primary stack, rail poles must be assumed independent and mutually coupled. Thus, the usual constraint from rotating machine analysis in which adjacent rotor poles of the same phase carry currents of equal magnitude and opposite polarity is removed. The result is a two-axis equivalent circuit in which each rail pole forms a current loop in each axis as shown in Fig. 1. The equivalent circuit formed by the pole-by-pole model may have any type of excitation, since no assumptions relating to the machine drive are made in the derivation. It is, therefore, a model well suited for analysis of transient behavior as well as operation from unbalanced voltages or inverter supplies rich in time harmonics.

Any existing LIM model is capable of simulating the steady-state performance of linear motors under the assumption of sinusoidal excitation. However, the pole-by-pole model appears to be the first approach to have the potential to simulate linear motor transient response. This advantage is attributed to the fact that most available models are based on steady-state electromagnetic field theory. Those few methods which can theoretically simulate transient conditions, such as Elliott's model [6], would either require hundreds of analog computer integrators or, quite possibly, days of digital computer time to do so. Clearly, few investigators would be inclined to pursue such an avenue even if they could afford the costs involved. Although the difficulties are formidable such results are certainly worth pursuing. Investigators who are presently exploring the application of linear motor drives to high-speed rail vehicles [9] find that acceleration and deceleration, effect of line voltage dips and supply faults, behavior with an inverter supply, dynamic stability, closed loop performance and many other conditions are of practical interest. In the past these problems could not be studied extensively, if at all, before a prototype was built. The pole-by-pole model makes analytical prediction of these conditions practical for the first time.

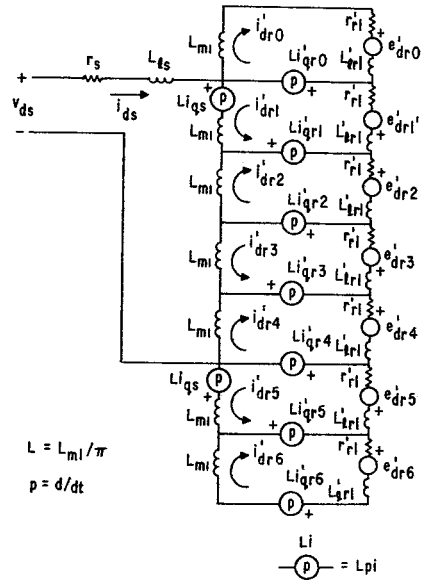

Fig. 1 d-axis equivalent circuit for a four pole linear induction motor modeled with seven rail poles.

In this paper the accuracy of the pole-by-pole model is first established by comparing predicted results to steady-state data taken from a test linear induction motor [8,9]. The analog computer representation of the pole-by-pole model is discussed and model-produced waveforms for sinusoidal voltage excitation will be shown for both steady-state and transient conditions. A simulation of a controlled current inverter (CCI) is then incorporated into the analog computer model and the steady-state simulation waveforms compared to the steady-state CCI drive waveforms measured from the actual machine. Lastly, waveforms resulting from step frequency changes, as measured from the test machine, will be compared to the waveforms generated by the analog computer model.

2. STEADY-STATE CONSIDERATIONS

Reference 1 presents a detailed derivation of the d,q axis pole-by-pole model and develops the equivalent circuit shown in Fig. 1 for a four pole test machine. One of the curves of the test machine which shows comparisons to steady-state model predictions is repeated herein as Fig. 2. It can be noted from Fig. 1

F79 199-1 A paper recommended and approved by the IEEE Rotating Machinery Committee of the IEEE Power Engineering Society for presentation at the IEEE PES Winter Meeting, New York, NY, February 4-9, 1979. Manuscript submitted September 5, 1978; made available for printing November 3, 1978.

0018-9510/79/0700-1366$00.75

that the model used to generate the solid curves has three more rail poles than primary poles. These extra poles have the function of modeling leading and trailing flux. It is important to mention that the number of poles in the model, seven, refers only to the number of rail poles. The primary is always modeled as physically wound (four poles). The values of the parameters in the equivalent circuit of Fig. 1 are derived from formulas similar to those used to analyze round machines [10] and are given in Table 1. This test machine was built as part of a Department of Transportation contract [8] and will also be used for purposes of comparison in this paper. The machine is rated 112 kW, has four poles occupying 43 slots and can simulate operation at up to 120 m/s, corresponding to synchronous speed for 300 Hz excitation. Thus, because end effects dominate performance, the machine cannot be accurately modeled by a conventional round rotor equivalent circuit [7].

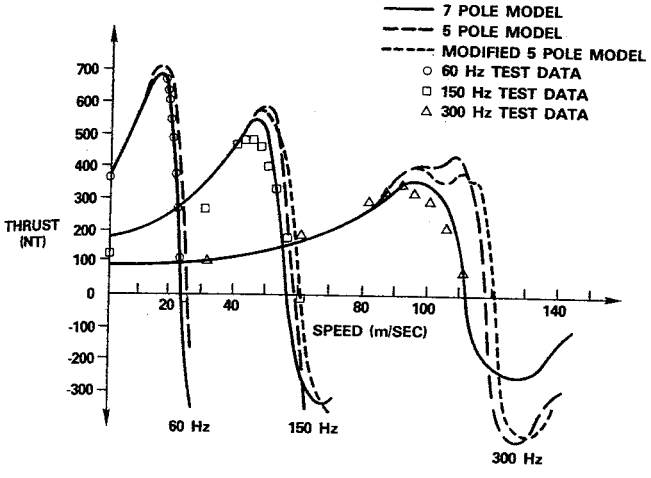

Fig. 2 Thrust vs. speed performance with 200 A. RMS stack current.

Table 1

Pole-by-Pole Model Machine Parameters
Reactances at 60 Hz

Parameter	Simulation Value
Primary Resistance, r_s	0.0174 Ω
Primary Leakage Reactance, $X_{\ell s}$	0.212 Ω
Mutual Reactance, X_m	0.3827 Ω
Secondary Resistance, r'_r	0.112 Ω
Secondary Leakage Reactance, $X'_{\ell r}$	0.0359 Ω

3. ANALOG SIMULATION OF POLE-BY-POLE MODEL

In previous work involving steady-state modeling it was determined that a model with seven effective rotor poles (14 sinusoidally distributed rotor windings) produces a good prediction of steady-state performance of the test machine [1]. Unfortunately, because of equipment limitations it was necessary to limit the present simulation to a model with one leading secondary winding, qr0, and one trailing winding, dr5, in addition to the eight secondary windings mandated by the primary windings as shown in Fig. 3. As a result the simulation is not presently able to account for the large trailing fluxes encountered at very high speeds, limiting its usefulness to speeds of about 80 meters per second (200 Hz excitation). Of course, the solution method to be outlined herein can be extended to any number of effective rotor poles. A simulation on a digital computer would experience no such equipment limitation. However, in view of the convenience and flexibility of the analog computer it was decided to proceed with an analog computer simulation. The long dashed line in Figure 2 shows the steady-state thrust speed curve for the reduced order model simulated in this paper. One can observe that the results are still quite satisfactory, in fact, even for 300 Hz excitation.

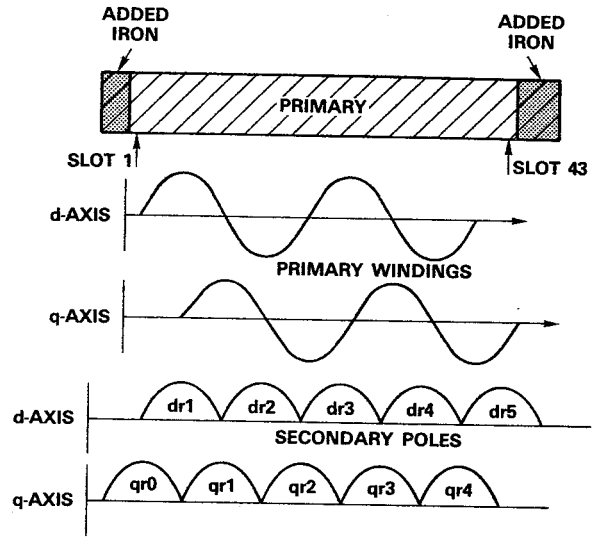

Fig. 3 Primary windings and secondary rail poles of pole-by-pole model simulated in this paper. Note added stack iron.

The pole-by-pole model for a linear induction motor, being similar in character to the equivalent circuit model for a round induction motor, may be simulated on an analog computer using round rotor machine simulation techniques [11]. Because of the similarity to round machines the derivation of the equations leading to the final analog computer diagram will not be presented in detail. Instead, it is sufficient to consider a representative equation describing one of the rotor poles, for example dr2. From Ref. 1 the equation which describes the flux linkages coupling rotor circuit dr2 is

$$\lambda'_{dr2}=L'_{\ell r1}i'_{dr2}+L_{m1}[i'_{dr2}-i_{ds}+(1/\pi)(i'_{qr1}+i'_{qr2})-8\bar{i}'_r/5\pi^2] \quad (1)$$

where i,L, and λ denote current, inductance and flux linkage respectively and

$$\bar{i}'_r = \text{sum of rail currents} = \sum_{k=0}^{5}(i'_{drk}+i'_{qrk})$$

and the subscripts are defined in Fig. 3. It is apparent that the term involving the sum of the rail currents, $\bar{i}'_r$, introduces many coupling terms between rail poles and, if left in the solution, would nearly double the number of potentiometers needed for the simulation. Fortunately, it has been verified that this term is generally very small. Hence, for simplicity it is assumed that

$$\bar{i}'_r = 0 \quad (2)$$

For comparison the short dashed curves of Fig. 2 show the accuracy of the five pole model with the effect of Eq. 2 included. It is seen that the simulation results are still reasonably accurate over a wide range of excitation frequencies and rail speeds.

Multiplying Eq. 1 (with $\bar{i}'_r = 0$) by a base frequency gives

$$\psi'_{dr2} = X'_{\ell r1} i'_{dr2} + X_{m1}[i'_{dr2} - i_{ds} + (1/\pi)(i'_{qr1} + i'_{qr2})] \quad (3)$$

where

$$\psi'_{dr2} = \omega_b \lambda'_{dr2}$$

$$X'_{\ell r1} = \omega_b L'_{\ell r1}$$

$$X_{m1} = \omega_b L_{m1}$$

and ω_b is a base or reference value of angular frequency.

Defining

$$\psi_{md2} = X_{m1}[i'_{dr2} - i_{ds} + (1/\pi)(i'_{qr1} + i'_{qr2})] \quad (4)$$

allows Eq. 3 to be expressed as

$$\psi'_{dr2} = X'_{\ell r1} i'_{dr2} + \psi_{md2}$$

Solving for i'_{dr2} yields

$$i'_{dr2} = (\psi'_{dr2} - \psi_{md2})/X'_{\ell r1} \quad (5)$$

Substituting Eq. 5 into Eq. 4 and rearranging gives

$$\psi_{md2} = \frac{X_{m1} X'_{\ell r1}}{X_{m1} + X'_{\ell r1}} [\psi'_{dr2}/X'_{\ell r1} - i_{ds} + (1/\pi)(i'_{qr1} + i'_{qr2})] \quad (6)$$

From Ref. 1 the voltage equation for rail pole dr2 is:

$$v'_{dr2} = r'_{r1} i'_{dr2} + d\lambda'_{dr2}/dt + \omega_r [L_{m1} i_{qs} + (L_{m1} + L'_{\ell r1})(i'_{qr1} - i'_{qr2})/2] \quad (7)$$

where v and r denote voltage and resistance and

ω_r = equivalent angular frequency = $\pi v/\tau$

where

v = vehicle speed

τ = pole pitch

The rightmost term in Eq. 7 is recognized as the speed voltage. Multiplying by ω_b and noting that all rail pole have no external excitation gives:

$$0 = \omega_b r'_{r1} i'_{dr2} + d\psi'_{dr2}/dt + \omega_r [X_{m1} i_{qs} + (X_{m1} + X'_{\ell r1})(i'_{qr1} - i'_{qr2})/2] \quad (8)$$

Substituting Eq. 5 into Eq. 8 and rearranging yields:

$$d\psi'_{dr2}/dt = -\omega_b r'_{r1}(\psi'_{dr2} - \psi_{md2})/X'_{\ell r1} - \omega_b e'_{dr2} \quad (9)$$

The quantity e'_{dr2} is the speed voltage term and is defined by comparison with Eq. 8. Integrating Eq. 9 gives:

$$\psi'_{dr2} = -\int [\omega_b r'_{r1}(\psi'_{dr2} - \psi_{md2})/X'_{\ell r1} + \omega_b e'_{dr2}] \, dt \quad (10)$$

Equations 5, 6, and 10 complete the analog computer simulation equations for secondary pole dr2. All other poles are handled in an identical manner. The final computer simulation diagram for a four pole machine is given in Figs. 4a, b and c. The simulation of the controlled current inverter used in many of the simulation runs is described in Ref. 12.

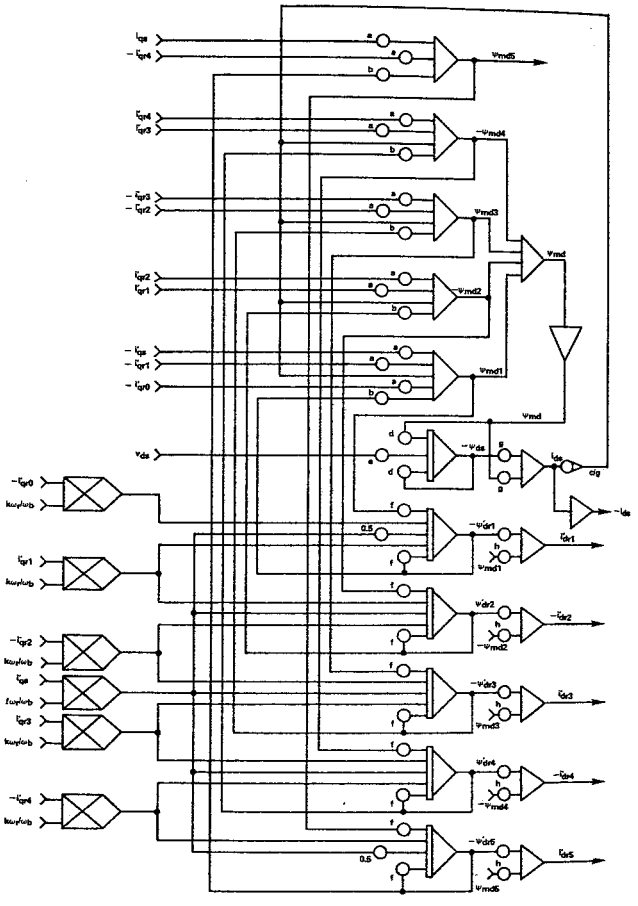

Fig. 4a Analog computer simulation diagram of d-axis circuit of four pole linear motor modeled with five rail poles.

4. ANALOG COMPUTER RESULTS WITH SINEWAVE VOLTAGE EXCITATION

In order to confirm the validity of the computer simulation developed in Section 3, tests were first performed with sinewave voltage excitation. Care was taken to display waveforms which are measurable quantities on the test machine. The flux linkage ψ_{dr1}, for example, can be measured by a flux coil spanning the first and ninth teeth (i.e. spanning the first pole pitch) of the primary stack. The rail current i_{dr1} can be measured by connecting two movable oscilloscope probes to a sidebar beside the first and ninth teeth (admittedly a difficult measurement) and observing the voltage drop across the constant sidebar resistance. The stack voltages and currents are easily measured by an oscilloscope. Thus the analog computer variables are most easily interpreted as the voltage equivalent of machine variables. Motion from left to right on the charts represents the passage of time.

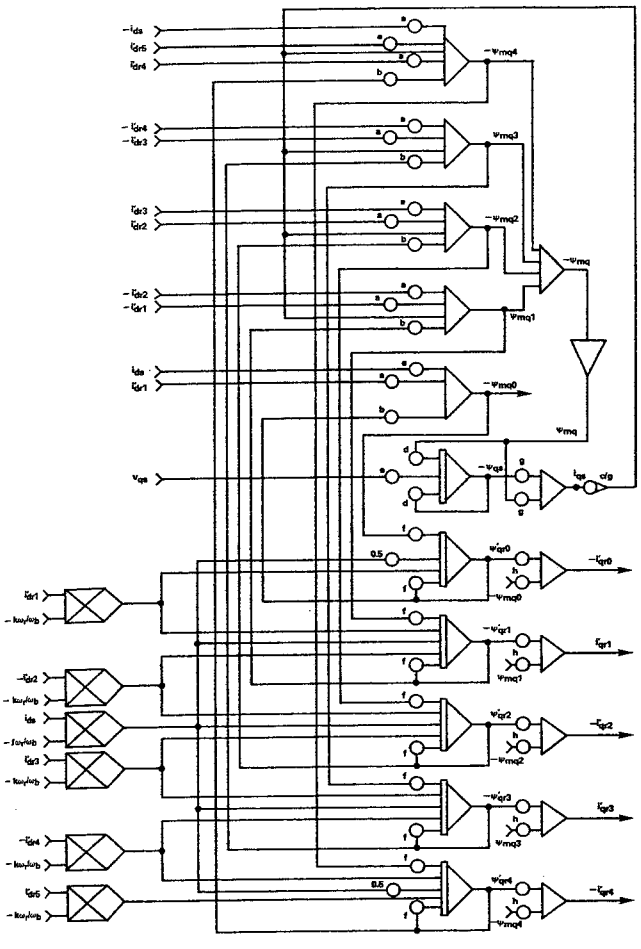

Fig. 4b Analog computer simulation diagram of q-axis circuit of four pole linear motor modeled with five rail poles.

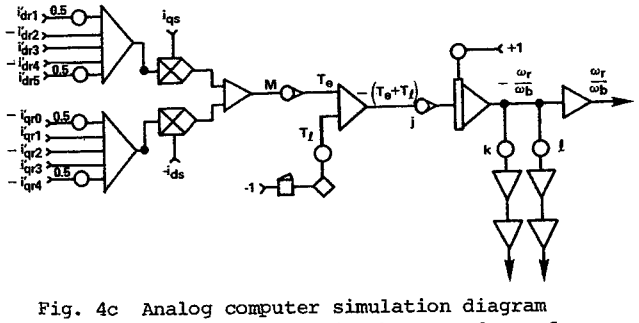

Fig. 4c Analog computer simulation diagram of electromagnetic thrust and speed.

The results given in Fig. 5 show the secondary mutual fluxes, thrusts, and speeds for zero, one-half and synchronous speed with 60 Hz sinewave voltage excitation. The results of Fig. 5 show the secondary currents, thrusts, and speeds for the same conditions. The 60 Hz flux waveforms of Fig. 5 show that at zero speed the four d-axis mutual fluxes, md1, md2, md3, and md4, directly under the primary windings are equal and opposite in phase angle while the others are nearly zero, as the case would be for a round machine. At synchronous speed however the mutual fluxes increase from the front pole, mq0, to the last pole under the primary, md4, then decrease in back of the machine. This result is clearly characteristic of linear motor behavior.

The 60 Hz secondary current distribution of Fig. 5 is especially interesting. At zero speed the four secondary currents under the primary windings, dr1, dr2, dr3, and dr4, are nearly equal and opposite in

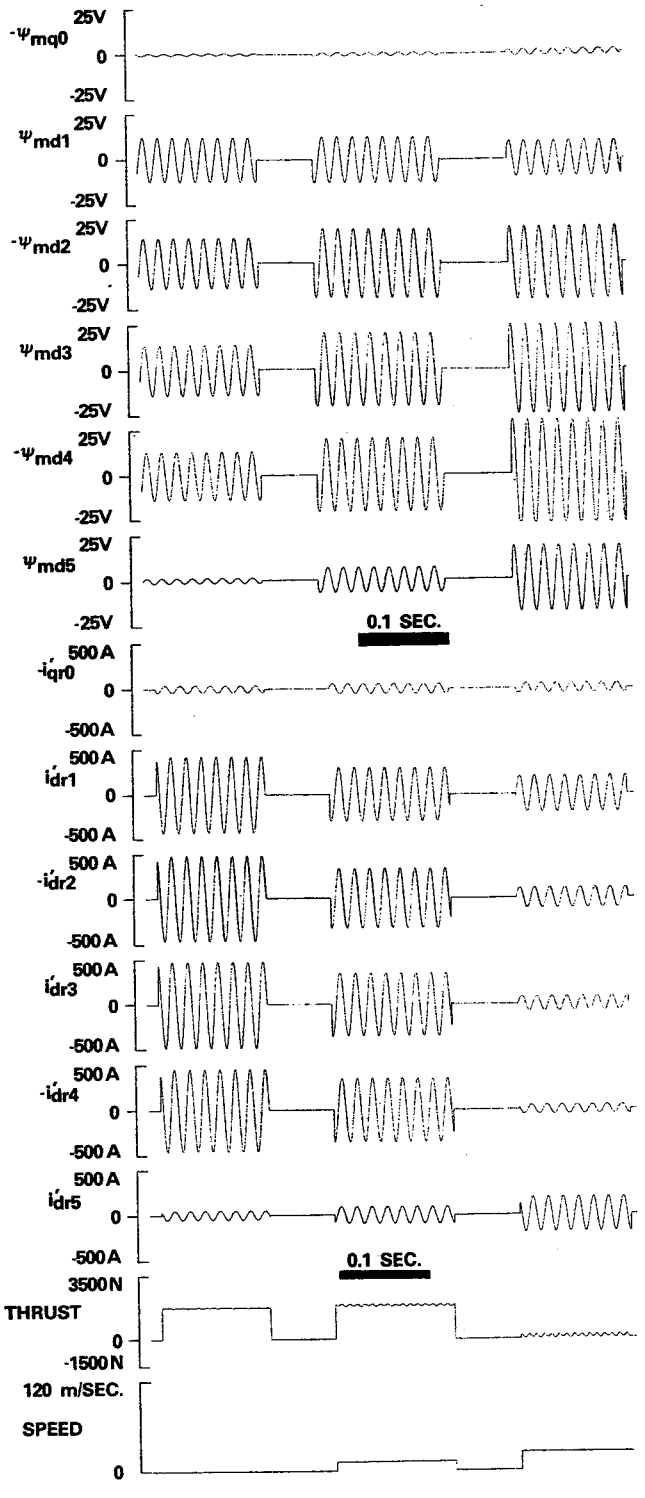

Fig. 5 Simulation traces of air gap fluxes and rail currents with 110 V, 60 Hz sinewave voltage excitation. Rail speed 0,12 and 24 m/s.

phase angle while the leading edge current, qr0, and trailing edge current, dr5, are much less. This again is indicative of round machine bahavior. However, at synchronous speed, only the current dr4 is tending toward zero while the others are quite large. This behavior is clearly different from that of round machine currents which uniformly approach zero at synchronous speed. The large currents in the front of the linear motor are needed to establish flux in the virgin secondary material entering under the primary while the large current behind the primary is caused by the decay of the now-established flux in the secondary material behind the primary.

The free acceleration trace of Fig. 6 was taken by suddenly applying a 150 Hz excitation voltage and allowing the machine to accelerate to full speed with no load. For convenience, reduced inertia was used to shorten the time needed to reach steady-state. These traces show the same trends as the steady-state traces with the addition of a redistribution of the fluxes back and forth in the air gap of the machine as speed increases. To the authors' knowledge such behavior has never previously been observed in linear machines. Also it is interesting to observe the double frequency (300Hz) torque pulsation which occurs as the the machine approaches synchronous speed. This behavior is a result of unbalanced line currents which flow due to the static end effect. Previous investigators have neglected this effect by assuming balanced sinusoidal currents in their analysis [2–6].

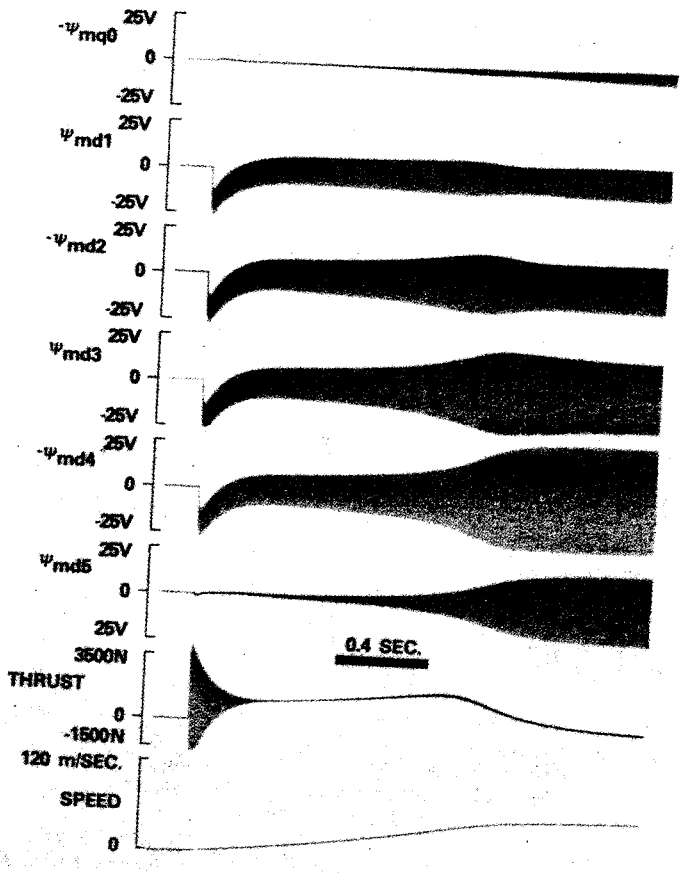

Fig. 6 Analog computer simulation results for free acceleration of linear motor. 550V, 300 Hz sinewave voltage excitation. Inertial set to 0.02 nominal.

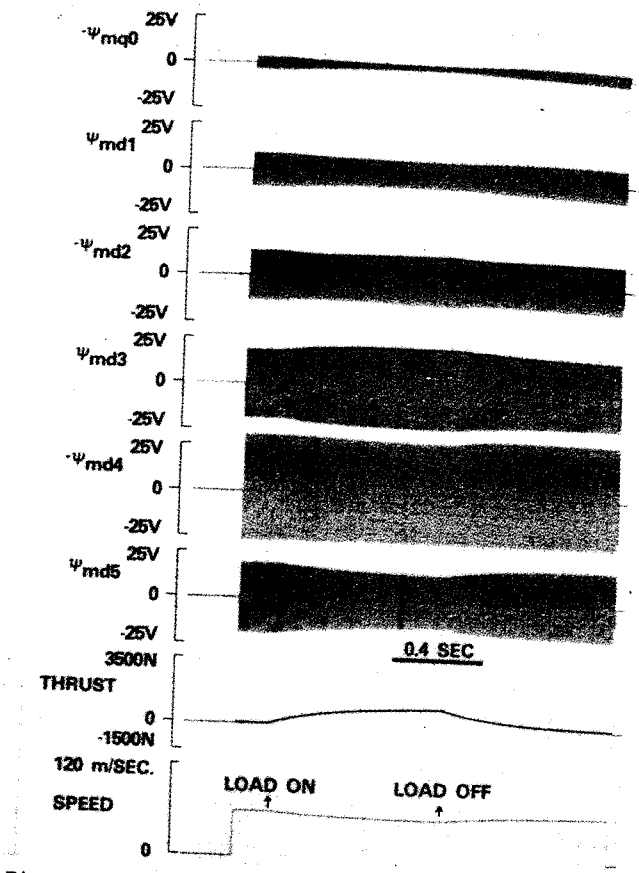

Fig. 7 Simulation traces for step load and unload of 1000 N from no-load condition. 275V 150 Hz sinewave voltage excitation, inertia set to 0.04 nominal.

The step load trace of Fig. 7 was taken by first allowing the motor to reach steady-state under no load conditions, applying a step thrust load of 1,000 newtons, again allowing steady-state to be reached, and finally suddenly removing the load. The secondary mutual flux and current traces again indicate a redistribution of flux in the machine as time progresses. Reduced inertia was again used to shorten the mechanical time constant of the system and allow steady-state to be reached in a reasonable number of cycles of the excitation frequency. In general these results indicated that the results of the analog computer simulation match very closely the steady-state results of the digital computer model [1]. It is also clear from Figs. 6 and 7 that the proper representation of transient behavior requires a complete computer simulation and could never be obtained from a simple quasi-steady-state model.

5. STEADY-STATE WAVEFORMS WITH CCI EXCITATION

The majority of the data points for the test machine were taken with a controlled current inverter (CCI) drive. Waveform data was recorded for the a-phase primary voltage and current, thrust, speed, and six of the flux search coils mounted on the primary stack of the machine during several of these runs to allow a comparison with simulation results. The voltage from the flux coils was integrated using a RC low pass filter with a cutoff frequency of 1.31 Hz. This approach allowed a direct reading of flux by the waveform recording instrumentation without the use of high cost chopper-stabilized operational amplifiers.

The left hand portion of Fig. 8 shows redrawn (to enhance readibility) oscilloscope photos of the flux coil voltages and the integral of these voltages during operation at 150 Hz and 200 Amps. The subscripts s7, s15, s25, etc. refer to the slot covered by a search coil; the sides of the search coil going along the center lines of two adjacent teeth. The spikes in the search coil are attributed to primary leakage fluxes coupling into the search coils, a likely assumption since the search coils are mounted only 0.76 mm above the surface of the primary.

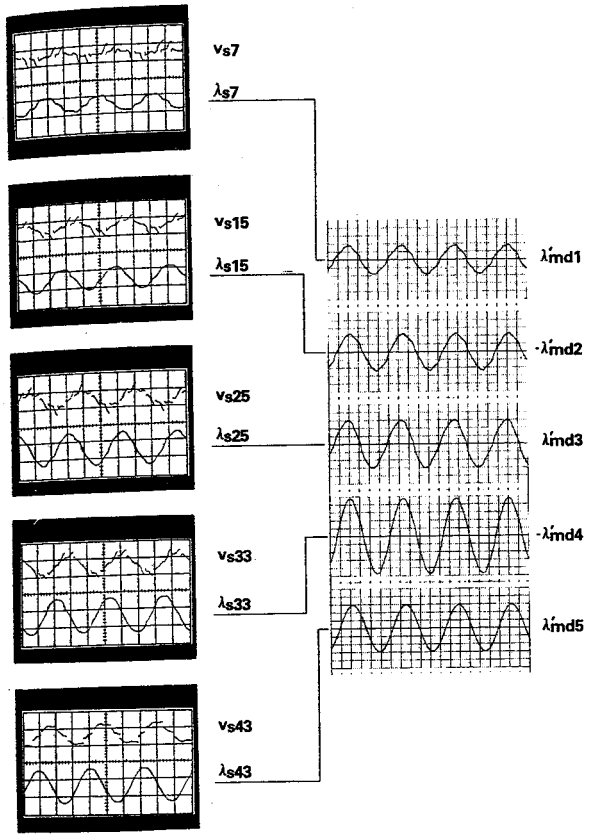

Fig. 8 Waveform comparison between measured air gap fluxes and simulation results. 150 Hz 200 A RMS CCI excitation at zero slip.

The lines connecting the search coil flux linkages with the analog computer traces on the right hand side of Fig. 8 show the correspondence between the sets of curves. Slot 7 is centered at pole md1, slot 15 at pole md2, slot 25 at pole md3, slot 33 at pole md4, and slot 43 at pole md5. The centering is one half slot pitch off in each case, an unavoidable consequence of having flux coils only at odd numbered slots. One can readily see that the magnitude and waveshape trends on either side of the connecting line are very much alike, slot 7 and pole md1 having the most distorted waveshapes in their groups, slot 43 and pole md5 having the most sinusoidal shapes in their groups, and corresponding traces having generally the same distortions. One must avoid looking for exact comparisons, however, since the photographs show the flux linkage over one slot pitch and the analog traces show the flux linkage over one pole pitch, nine times larger. Still, the comparisons show the trends seen in the actual machine are well represented in the analog simulation.

The waveforms of Fig. 9 compare the analog computer traces on the left to the visicorder (lightbeam galvanometer) recording of the test machine waveforms on the right. The excitation frequency is 60 Hz at 200

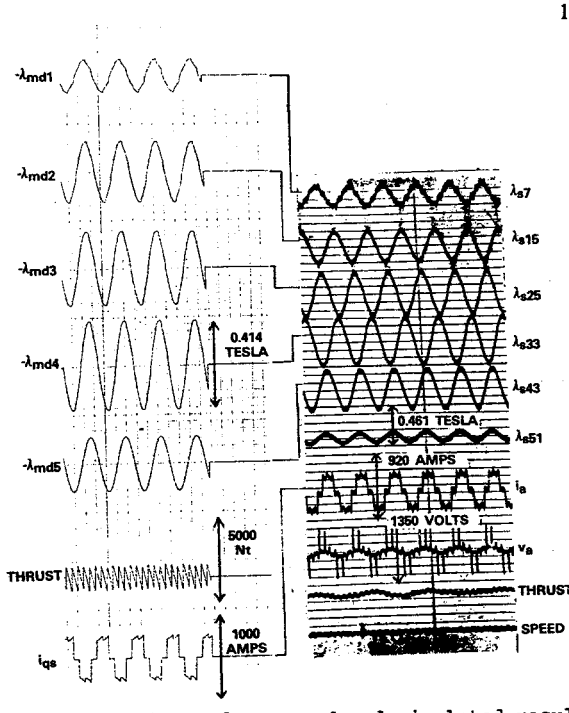

Fig. 9 Comparison of measured and simulated results for 60 Hz, 24 m/s operation with CCI supply. All flux linkages are referred to equivalent flux densities.

amperes RMS per phase and the speed is 24 m/s. This figure again shows the analog computer traces are similar to those recorded directly from the machine. The current waveforms of the analog and visicorder traces vary slightly because an ideal rectifier (no ripple voltage) was assumed for the simulation. The speed signal on the visicorder traces was obtained from a Himmelstein torque transducer and the thrust trace was from a force sensor attached to the primary of the LIM.

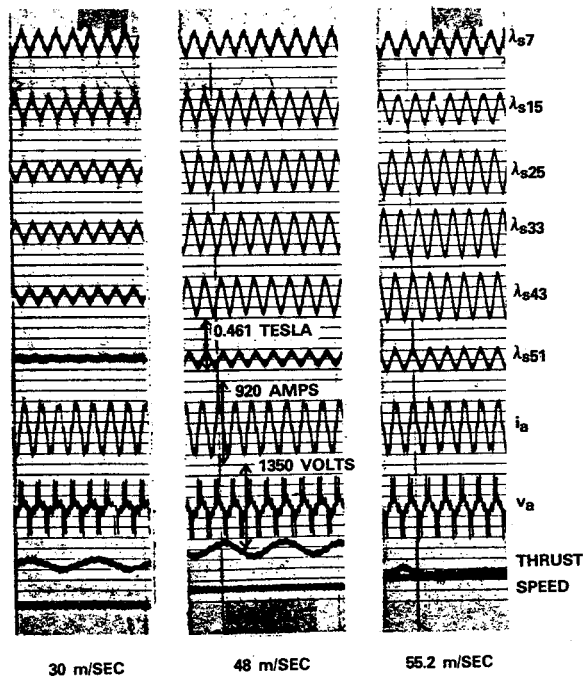

Fig. 10 Measured waveforms with 150 Hz CCI excitation at 50%, 20% and 8% slip. Flux linkages are referred to equivalent flux densities.

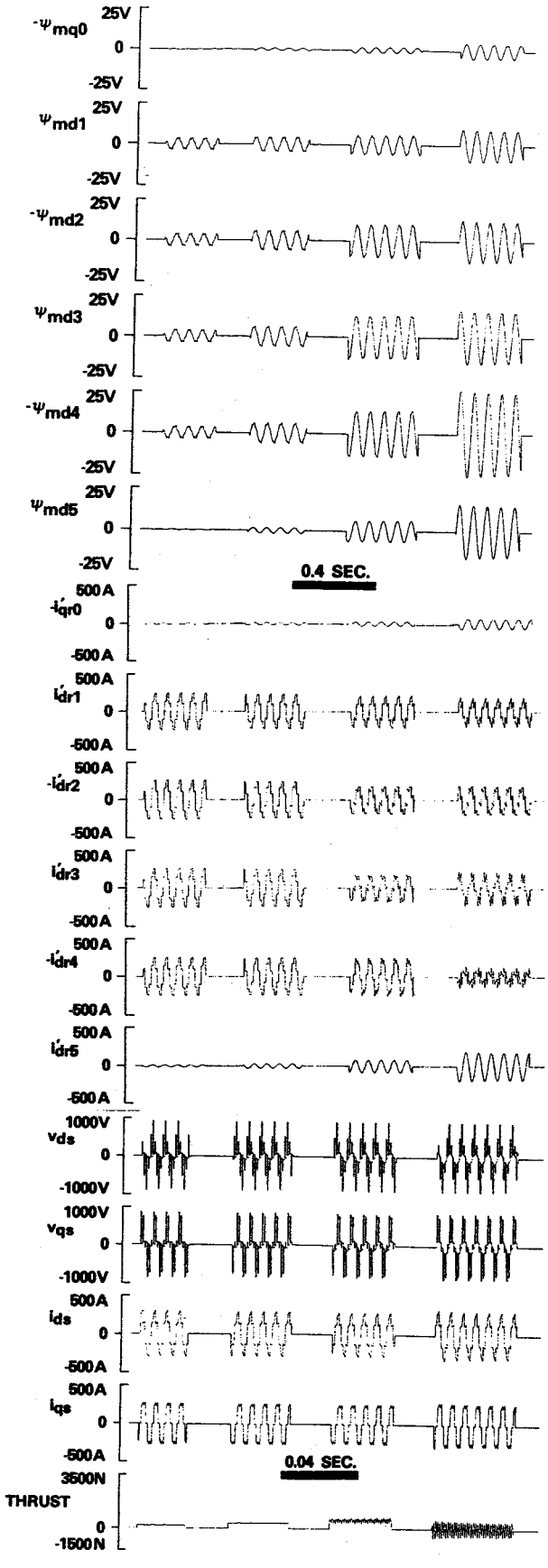

Fig. 11 Calculated fluxes, currents, voltages and thrust for 200 A RMS, 150 Hz CCI excitation. Rail speeds 0, 30, 48 and 60m/s left to right.

The waveforms of Fig. 10 were taken at 50%, 20%, and 8% slip with 150 Hz, 200 Amp CCI excitation and show the changes in the fluxes of the test machine as speed changes. Figure 11 shows steady-state 150 Hz analog computer traces at 100%, 50%, 20%, and 0% slip with 200 Amp CCI excitation. It is interesting to observe the increase in the fundamental of the excitation voltage as speed and frequency increase and the nearly sinusoidal shape of the trailing secondary current i_{dr5}.

6. TRANSIENT WAVEFORMS WITH CCI DRIVE

Although space constraints prohibit a full documentation of all tests, numerous types of transients were recorded and compared with simulation results including step load changes, sudden energization and step changes in control variables. Probably the most significant transient encountered in this study was the effect of a step change in inverter frequency. Figure 12 shows test machine waveforms for a 150 to 90 Hz freqency step change at 45 meters per second (approx. −20% slip to +20% slip). This trace shows the inverter current and mutual fluxes more than doubling after the change is introduced. The same result is seen in the analog simulation of Fig. 13. Note that the thrust of Fig. 13 has a negative peak at -6000 newtons. This is 6 times rated thrust at half rated current. Figure 12 shows this effect to a lesser degree because of the damping of the primary to which the force sensors are attached.

A more drastic type of transient is simulated in Fig. 14. The speed is set to 48 m/s at an excitation frequency of 150 Hz when the switch simulating the negative a-phase SCR is turned off, modeling an open circuit failure. Note that the mutual fluxes respond very quickly to this change, illustrating the fast electrical time constant of the machine. Those readers interested in an extensive treatment of the waveform data are encouraged to consult Ref. 10.

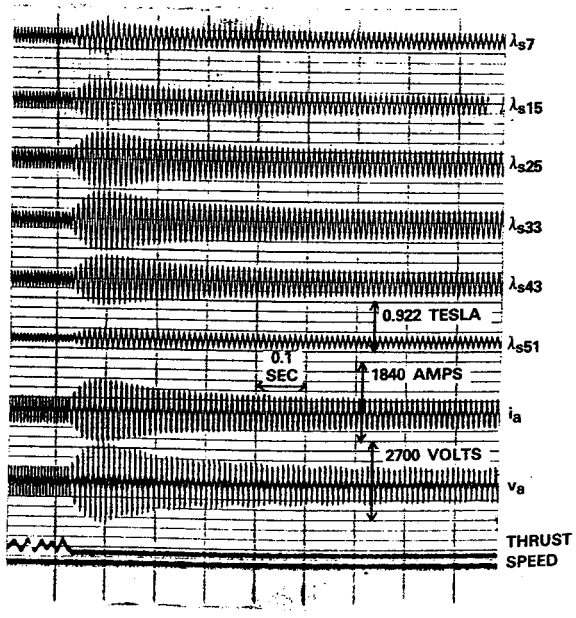

Fig. 12 Measured waveforms of the tested machine for a 150 Hz to 90 Az step change in frequency at 45 m/s. All flux linkages referred to equivalent flux densities. Thrust sensor reads only positive values.

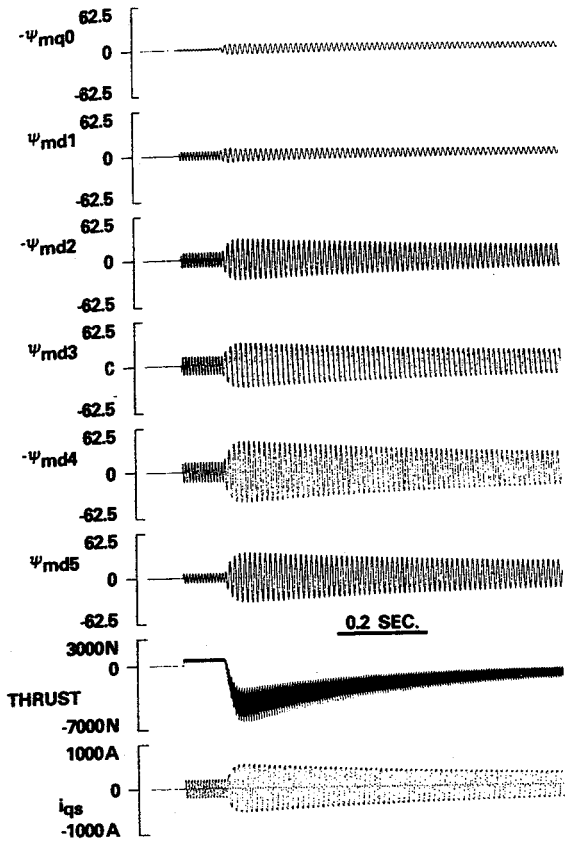

Fig. 13 Computer traces for the simulated machine with the same 150-90 Hz change in frequency as Fig. 12. Regulator time constant is 250 ms.

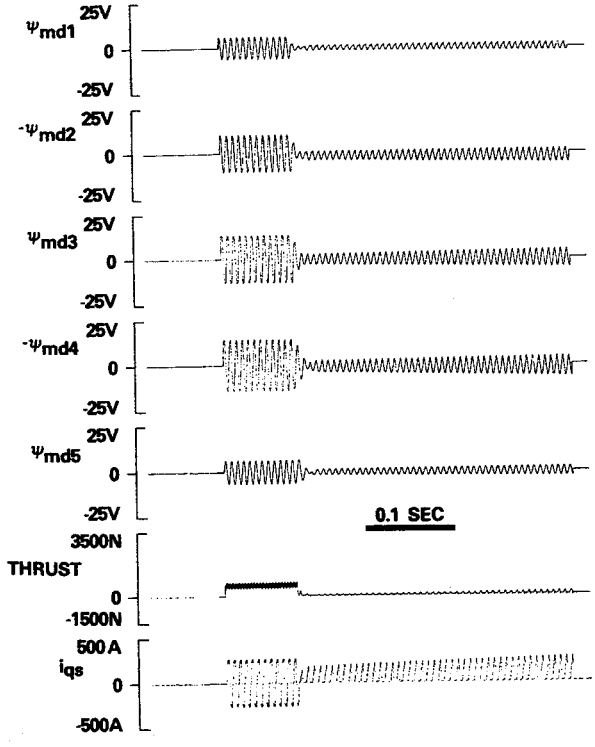

Fig. 14 Computed performance of linear motor for a thyristor failure in the current source inverter. Operation at 150 Hz,200A, 48 m/s.

7. CONCLUSION

This paper has demonstrated that the pole-by-pole model for a linear induction motor, in addition to giving good steady-state sinewave excitation results, is capable of accurately simulating the response of a linear machine to non-sinusoidal excitation and transient conditions. These last two features are, at this time, beyond the practical capabilities of any other analysis procedure and make the pole-by-pole model a highly-valuable addition to linear motor theory.

8. ACKNOWLEDGEMENT

This work was supported by the Federal Railroad Administration under contract No. DOT-FR-64147. The authors wish to thank W.R. Oney and W.R. Mischler the engineers in charge of taking data for the test machine. Their explanations of the test facilities, and those of D. Evans, greatly aided the work of instrumenting the LIM for waveform measurement. The authors also wish to thank Mr. M. Guarino Jr. for his encouragement and support.

9. REFERENCES

(1) T.A. Lipo and T.A. Nondahl, "Pole-by-Pole d-q Model of a Linear Induction Machine," Paper No. F78 317-0, 1978 IEEE PES Winter Power Meeting.

(2) S. Yamamura and H. Ito, "Three-Dimensional Analysis of Linear Induction Motors," 1976 IEEE-IAS Annual Meeting Conference Record, pp. 1180-1187.

(3) H. Mosebach, "Effect of Finite Length and Width on Short Stator and Short Rotor Linear Motors," PhD Dissertation, Tech. Univ. Braunschweig, May 1972 (In German).

(4) K. Oberretl, "Three-Dimensional Analysis of Linear Induction Motor Taking Account of Edge-Effects and the Distribution of the Winding," Arc. f. Elek. vol. 55, pp. 181-190, April 1973 (In German).

(5) B.-T. Ooi, "A Generalized Machine Theory of the Linear Motor," IEEE Trans. Power App. & Sys., vol. PAS-92, pp. 1252-1259, Jul/Aug 1973.

(6) D.G. Elliott, "Matrix Analysis of Linear Induction Machines," Report No. FRA-OR&D-75-77, U.S. Dept. of Transportation, 330 pp., Sept. 1975.

(7) P.L. Alger, Induction Machines, Their Behavior and Uses, (Gordon and Breach: New York), 1970.

(8) G.B. Kliman, W.R. Mischler and W.R. Oney,"Performance of a Single-Sided Linear Induction Motor with Solid Back Iron and with Various Misalignments," Report No. FRA/ORD-78-36, U.S. Dept. of Transportation, 651 pp., May 1978.

(9) W.R. Oney and W.R. Mischler, "Experimental Evaluation of a High Speed Single Sided Linear Induction Motor," Paper No. A78 278-4, 1978 IEEE PES Winter Power Meeting.

(10) T.A. Nondahl, "Steady-State and Transient Analysis of a Short Primary Linear Induction Motor Using a d-q Axis Pole-by-Pole Model," PhD Dissertation, Univ. of Wisconsin-Msn., Dec 1977.

(11) P.C. Krause and C.H. Thomas, "Simulation of Symmetrical Induction Machinery," IEEE Trans. Power App.& Sys., vol. PAS-84, pp. 1038-1053, Nov. 1965.

(12) T.A. Lipo, "Simulation of a Current Source Inverter Drive," Power Electronics Specialists Conference, Palo Alto, CA, June 14-16, 1977, IEEE Pub. No. 77CH 1213-8 AES, pp. 310-315.

10. NOMENCLATURE AND SYMBOLS PERTAINING TO FIG. 4

Analog Diagram Symbol	Definition or Equation	Value
M	Mass	850 kg
T_e	Electromagnetic Thrust	
T_ℓ	Load Thrust	
v_b	Base Speed	24 m/s
ω_r	Equivalent Rotor Angular Velocity or $\pi v/\tau$	
ω_b	Base Frequency	377 Rad/s
τ	Pole Pitch	0.2002 m
r_s	Primary Resistance	0.0174 Ω
r'_{rl}	Per-Pole Secondary Resistance	0.028 Ω
$X_{\ell s}$	60 Hz Primary Leakage Reactance	0.212 Ω
$X'_{\ell rl}$	Per-Pole 60 Hz Secondary Leakage Reactance	0.00898 Ω
X_{ml}	Per-Pole 60 Hz Mutual Reactance	0.09568 Ω
X^*_{ml}	$[(1/X_{ml}) + (1/X'_{\ell rl})]^{-1}$	0.008209 Ω
a_t	Time Scale	200
a	X^*_{ml}/π	0.002613
b	$X^*_{ml}/X'_{\ell rl}$	0.9142
c	$X^*_{ml}/X_{\ell s}$	0.03872
d	$\omega_b r_s/(X_{\ell s} a_t)$	0.1547
e	ω_b/a_t	1.885
f	$\omega_b r'_{rl}/(X'_{\ell rl} a_t)$	5.878
g	$1/X_{\ell s}$	4.717
h	$1/X'_{\ell rl}$	111.4
j	$1/(a_t M v_b)$	$2.45 \cdot 10^{-7}$
k	$(\omega_b/a_t) X_{ml}$	0.1804
ℓ	$(\omega_b/a_t)(X_{ml} + X'_{\ell rl})/2$	0.09864

11. APPENDIX 1 ANALOG COMPUTER SYMBOLS

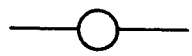
Potentiometer (non-sign inverting)


Potentiometer (sign inverting)

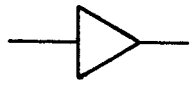
Inverter/Summer (sign inverting)


Integrator (sign inverting)

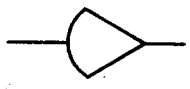
High Gain Amplifier (sign inverting)


Limiter

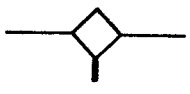
Logic Controlled SPST Analog Switch


Analog Comparator with Logic Output